# FUNDAMENTAL PROCESSES IN THE EXPANSION, ENERGIZATION, AND COUPLING OF SINGLE- AND MULTI- ION PLASMAS IN SPACE: LABORATORY SIMULATION EXPERIMENTS

SAIC Final Report 96/1157
July 1, 1996
NASW-4652

**Science Applications International Corporation**

*An Employee-Owned Company*

*1710 Goodridge Drive, P.O. Box 1303, McLean, Virginia 22102 (703) 821-4300*

*Other SAIC Offices: Albuquerque, Boston, Colorado Springs, Dayton, Huntsville, Las Vegas, Los Angeles, Oak Ridge, Orlando, Palo Alto, San Diego, Seattle, and Tucson*

# FUNDAMENTAL PROCESSES IN THE EXPANSION, ENERGIZATION, AND COUPLING OF SINGLE- AND MULTI- ION PLASMAS IN SPACE: LABORATORY SIMULATION EXPERIMENTS

SAIC Final Report 96/1157
July 1, 1996
NASW-4652

Prepared by

E.P. Szuszczewicz and T.T. Bateman

Laboratory for Atmospheric and Space Science
Science Applications International Corporation
McLean, VA 22102

RPT-97-18

NASA National Aeronautics and Space Administration

# Report Documentation Page

| 1. Report No. | 2. Government Accession No. | 3. Recipient's Catalog No. |
|---|---|---|
| | | |

**4. Title and Subtitle**

Fundamental Processes in the Expansion, Energization, and Coupling of Single- and Multi-Ion Plasmas in Space: Laboratory Simulation Experiments

**5. Report Date**

7/1/96

**6. Performing Organization Code**

**7. Author(s)**

E.P. Szuszczewicz and T.T. Bateman

**8. Performing Organization Report No.**

**10. Work Unit No.**

**9. Performing Organization Name and Address**

Science Applications International Corporation
1710 Goodridge Drive
McLean, VA 22102

**11. Contract or Grant No.**

NASW-4652

**12. Sponsoring Agency Name and Address**

National Aeronautic and Space Administration
Washington, DC 20546

**13. Type of Report and Period Covered**

Final

**14. Sponsoring Agency Code**

**15. Supplementary Notes**

**16. Abstract**

We have conducted a laboratory investigation into the physics of plasma expansions and their associated energization processes. We studied single- and multi-ion plasma processes in self-expansions, and included light and heavy ions and heavy/light mixtures to encompass the phenomenological regimes of the solar and polar winds and the AMPTE and CRRES chemical release programs. The laboratory experiments provided spatially-distributed time-dependent measurements of total plasma density, temperature, and density fluctuation power spectra with the data confirming the long-theorized electron energization process in an expanding cloud - a result that was impossible to determine in spaceborne experiments (as e.g., in the CRRES program). These results provided the missing link in previous laboratory and spaceborne programs, confirming important elements in our understanding of such solar-terrestrial processes as manifested in expanding plasmas in the solar wind (e.g., CMEs) and in ionospheric outflow in plasmaspheric fluxtube refilling after a storm. The energization signatures were seen in an entire series of runs that varied the ion species ($Ar^+$, $Xe^+$, $Kr^+$ and $Ne^+$), and correlative studies included spectral analyses of electrostatic waves collocated with the energized electron distributions. In all cases wave energies were most intense during the times in which the suprathermal populations were present, with wave intensity increasing with the intensity of the suprathermal electron population. This is consistent with theoretical expectations wherein the energization process is directly attributable to wave particle interactions. No resonance conditions were observed, in an overall framework in which the general wave characteristics were broadband with power decreasing with increasing frequency.

| 17. Key Words (Suggested by Author(s)) | 18. Distribution Statement |
|---|---|
| Laboratory Experiments, Plasma Expansions, Space Simulations, Electron Energization | |

| 19. Security Classif. (of this report) | 20. Security Classif. (of this page) | 21. No. of pages | 22. Price |
|---|---|---|---|
| Unclassified | Unclassified | | |

## TABLE OF CONTENTS

## 1. EXECUTIVE SUMMARY

We have conducted a laboratory investigation into the physics of plasma expansions and their associated energization processes. Supported by a numerical modelling activity, the expansion and coupling processes were studied for their own intrinsic value, for their relationship to equivalent processes in the solar-terrestrial system, and for their importance to NASA programs involving chemical release experiments in space. We studied single- and multi-ion plasma processes in self-expansions. We included light and heavy ions and heavy/light mixtures to encompass the phenomenological regimes of the solar and polar winds and the AMPTE and CRRES chemical release programs. And we provided spatially-distributed time-dependent measurements of total plasma density, temperature, and density fluctuation power spectra.

The experiments were conducted in unique facilities with diagnostic tools that: (1) explored the fundamental cause-effect relationships in early-time plasma expansion and coupling processes; (2) quantified the temporal and spatial distributions of suprathermal forerunner plasma particles and related the energy gained by the forerunners to the electron temperature in the expanding gasses; and (3) verified the presence of shock-like structures and studied the particle and wave characteristics in and through the shock.

The data confirmed the long-theorized electron energization process in an expanding cloud-a result that was impossible to determine in spaceborne experiments (as e.g., in the CRRES program). These results provided the missing piece to previous laboratory and spaceborne programs, confirming important elements in our understanding of such solar-terrestrial processes as manifested in expanding plasmas in the solar wind (e.g. CMEs) and in ionospheric outflow in plasmaspheric fluctuate refilling after a storm.

The energization signatures were seen in an entire series of runs that varied the ion species ($Ar^+$, $Xe^+$, $Kr^+$ and $Ne^+$). And correlative studies included spectral analyses of electrostatic waves collocated with the electron tail distributions. In all cases wave energies were most intense during the times in which the suprathermal populations were present, with wave intensity increasing with the intensity of the suprathermal electron population. This is in keeping with theoretical expectations wherein the energization process was directly attributable to wave particle interactions. No resonance conditions (i.e., in terms of wave frequencies) were observed. The general characteristics were broadband with power decreasing with increasing frequency

## 2. SPACE SCIENCE PERSPECTIVES ON EXPANDING PLASMAS

The basic principles of plasma expansions and their interactions with local particle populations and fields are fundamental to the concept of transfer of energy and mass in the Sun-Earth system. Solar and heliospheric physics seek

to understand mass and energy transport in and through the photosphere and the associated interactions of convective plasma flows and magnetic fields. Stretching outward from the Sun, the space plasma emphasis is on acceleration processes and the transport of energy, mass and magnetic fields, including the evolution and structure of the solar wind. Closer to the Earth, specific interests focus on solar wind-magnetosphere interactions, ionospheric-magnetospheric coupling, the expanding polar wind and interhemispheric plasma flows. There is little doubt that few phenomena span such a wide range of solar-terrestrial applications as expanding plasmas and their attendant energization and interaction processes.

This investigation contributed to this important aspect of solar-terrestrial research, not in the sense that our laboratory experiments were rigorous simulations of the varied phenomenological domains, but in the sense that our experiments and modelling activity addressed the fundamental components of the overall process, and allowed for flexibility in parameter controls and time-resolved multi-parameter diagnostics. The resulting physics and improved specifications complement and extrapolate the one-dimensional domain of satellite and rocket observations of expanding plasma interactions, and allow for a more rigorous and accurate interpretation of the "in situ" spaceborne results.

The subject of plasma expansion, convection, acceleration and associated coupling processes in solar-terrestrial and laboratory environments has had a number of recent reviews that help put the overall problem in perspective.[1-5] Reduced to a simple summary statement it can be said that space plasma processes influenced by expansion and coupling mechanisms include: (1) solar flares and coronal mass ejections, (2) the interplanetary medium and solar wind, (3) the bowshock and magnetotail, (4) magnetosphere-ionosphere interactions resulting in auroral zone acceleration mechanisms, and (5) the depletion and refilling of fluxtubes during magnetospheric substorms. Regardless of the view, all investigations raise similar questions regarding the basic physics:[2]

(1) *What are the characteristics of the source plasma and its particle and field distributions? How do these characteristics influence the evolution of the expansion process itself?*

(2) *What are the physical conditions in the acceleration region, and what are the consequences of the acceptation process on the composition, velocity distribution, associated anisotropies and time dependence of the products of the expansion and acceleration process?*

(3) *What are the characteristics of the acceleration mechanism itself? What are the amplitudes of electric field fluctuations and the efficiency with which a given acceleration process operates?*

(4) *What are the sources of free energy in the system and how do the energy and momentum in the expanding plasma couple to the local magnetic field and background plasma?*

Developing answers to this set of questions represents an important scientific challenge. This is especially true in the practical world of space observations where we find: (1) a rather large difference in observational techniques, instrument complements and data acquisition rates, (2) limitations imposed by the along-track one-dimensionality of satellite and rocket measurements that cause ambiguities in separating spatial variations from those of a temporal nature, (3) the lack of multi-point, multi-parameter time-resolved diagnostics, and (4) the inability to execute parametric controls that would provide a definitive test and validation of an observation and its associated interpretation. The result is a non-trivial task to identify a spaceborne observation with a specific mechanism and the attendant coupling to the background environment.

We illustrate the difficulties in spaceborne investigations with reference to Figures 1 and 2. In Figure 1A we present the experiment scenario for the TOR rocket investigation.[31a] It was designed to study the ionospheric-magnetospheric response to a sudden ionospheric disturbance at low altitudes and to test ionospheric generator mechanisms of cross-field ion drag by neutrals and current closure across auroral forms.[31a,b] The experiment was conducted at a high-latitude site, releasing two cesium clouds on the downleg portion of the trajectory at 171 and 110km, respectively. In release #1 (see Figure 1A) a large amplitude electric field pulse was detected near the leading edge of the expanding cloud, and a simple three dimensional model was developed to explain the results. The pictorial representation of that model, illustrated in Figure 1B, shows the relative position of the cloud center with respect to the diagnostics payload in a reference system with $\vec{B} \parallel \hat{z}$. The model details are not important here. What is important, however, is that *with a single point measurement where the expansion front of the cloud was crossing the magnetic field at an obtuse angle, the interpretation of the observation required the development of a model to describe not only the time-dependent electric field distribution but the three-dimensional current system in the cloud with closure through ionospheric paths.* This problem of limited data support for accurate interpretations is not uncommon in active space experiments. For example, very similar circumstances prevailed in AMPTE observations of shocklike electrostatic noise in a solar wind chemical release. The analysis of AMPTE data suggested that the shocklike noise could be generated by one of two instabilities, but the investigators were unable to determine which instability was actually dominant due to lack of information on the wave propagation direction and the temperature of the cold electrons.[34b]

The difficulties also prevailed in the CRRES program. CRRES carried a complement of chemical canisters to be released in the Earth's ionosphere and magnetosphere. The release scenarios were designed: (1) to study low-latitude

electric fields and the transport of ions along magnetic field lines to the conjugate ionosphere, (2) to study momentum coupling between the injected plasma and the background ionosphere, (3) to study the critical ionization hypothesis by cloud injection at orbital velocities, and (4) to simulate and test plasma expansion processes that are expected to be operating in the polar wind and in interhemispheric plasma flows after substorms. In one form or another these objectives involved momentum and energy coupling to the background plasma and the local geomagnetic field. Not only did CRRES not have multi-point measurements but its diagnostics complement and sampling rate were limited in temporal and spatial resolution. To unfold the details of energy and momentum coupling means time-resolved, three-dimensional measurements of particles and fields covering the very earliest time of cloud injection (10's of milliseconds) to the point at which it reaches dynamic equilibrium with the background ionosphere ($\approx$ 10's of seconds). CRRES release scenarios had no capability to investigate the complete spectrum of time-dependent coupling regimes, and were in fact limited to the timeframe after the cloud had undergone its formidable stages of continuum and transition flows. These early phases define the cloud's neutral and charged particle distributions as they enter the final regime of collisionless expansion.

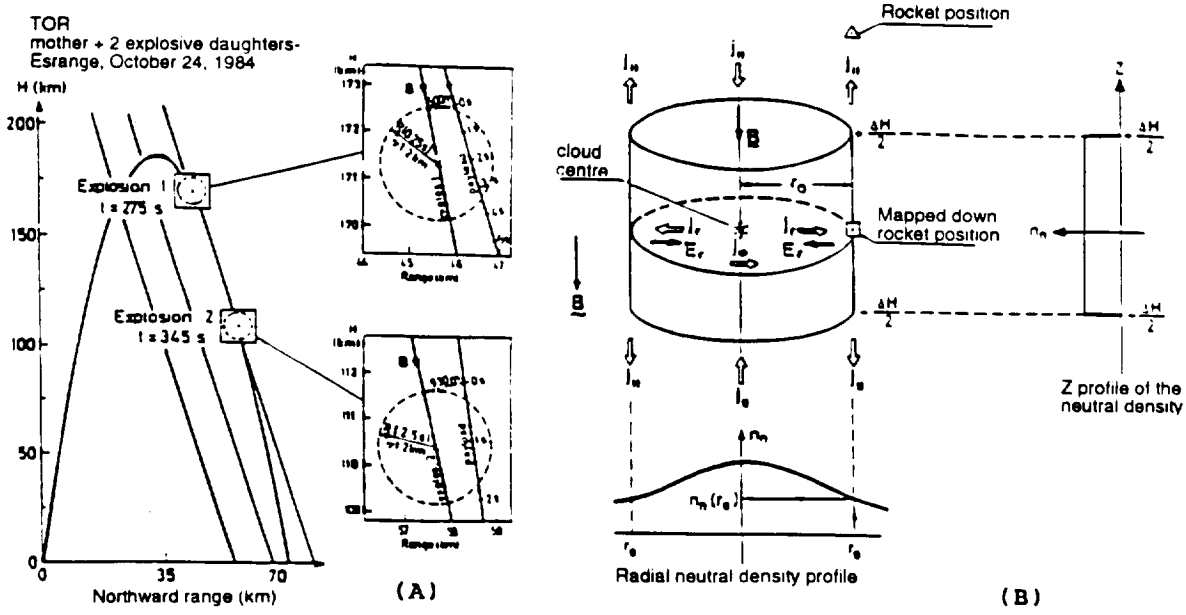


***Figure 1.*** *(A) Trajectory plot for the TOR chemical release experiment. Inserts show the detail geometric relationship between the clouds and the payload trajectory at explosion time. (B) Schematic illustration of expanding cloud model (a truncated cylinder) showing the position of the rocket with respect to the cloud center in a reference system with* $\vec{B} \parallel \hat{z}$. *For explosion 1, the position of the rocket, mapped down into the plane that includes the cloud center and is perpendicular to* $\vec{B}$, *is at a radius* $r_o$=500m. *(Adapted from Marklund, et al.*[31]*)*

The CRRES scenario illustrated in Figure 2 can be considered typical, in that the expanding cloud and satellite approached each other at some angle relative to the local magnetic field. In zero-order, the neutrals tend to have a spherically symmetric distribution while the plasma components are strongly anisotropic. The spacecraft makes a one-dimensional pass through the time- and spatially-dependent expanding cloud and forms a database that is inadequate to uniquely unfold the anistropic and three-dimensional aspects of the expansion and coupling process.

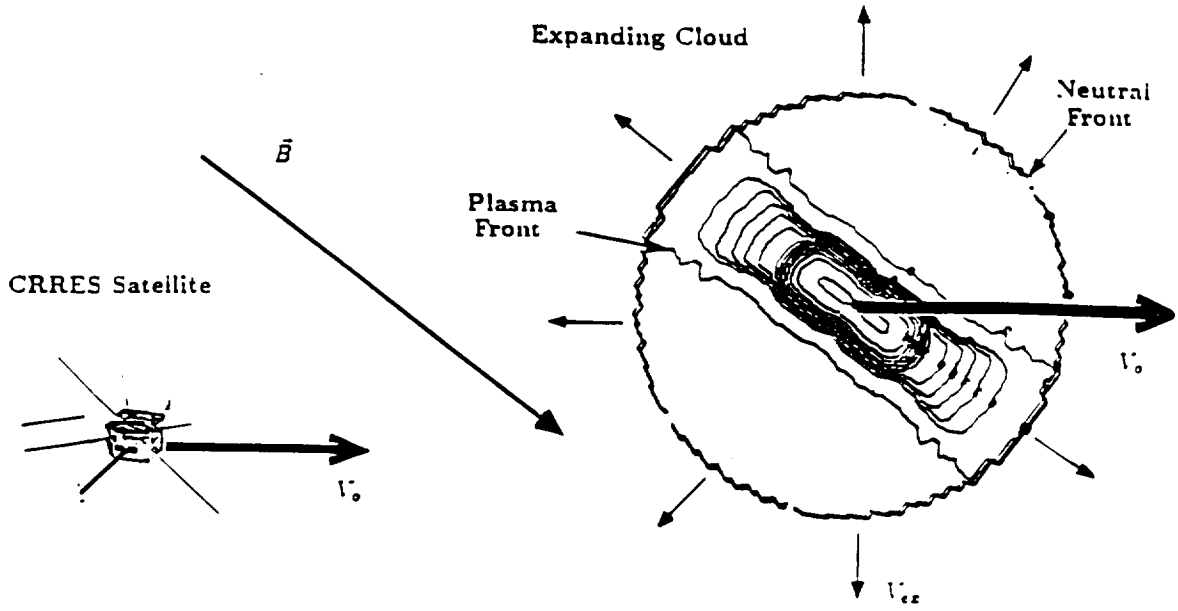


***Figure 2.*** *Illustration of a CRRES chemical release experiment scenario. The figure has been drawn to bring attention to the zero-order expansion process in which a point source will have neutrals expanding isotropically while the plasma expansion has the anisotropic control of the ambient* $\vec{B}$ *-field.*

This is a scenario not unfamiliar to spaceborne investigators. But the situation is better in the study of natural processes (e.g. particle precipitation patterns in the auroral zone) where a satellite mission can normally accumulate more than $1.5(10^9)$ kbits of data over a three-year mission. This allows many revisits of an observed phenomena, with an opportunity to identify trends in nominal and transient processes and to develop a self-consistent model for the observations. Assuming as much as 50 seconds as representative of the early-time coupling process, the total "in situ" observational time for all 24 CRRES releases was of the order of 20 minutes with a total accumulated data of $1.9(10^4)$ kbits.

In the following sections we review many of the physical mechanisms expected to be operating in expansion processes. This will involve acceleration, particle energization, attendant particle-field interactions and ion mass discrimination effects. The discussion will expose the complexity of the overall problem and

establish the measurement requirements that must be met in any related experimental investigation. We will then establish an important identity between microscale and macroscale expansion phenemenologies and the associated relevance of laboratory simulations to the spaceborne counterparts.

## 3. PLASMA EXPANSION PROCESSES AND MANIFESTATIONS OF COUPLING

### 3.1 The Fundamental Expansion Process

**3.1.1 Basic Concepts**. Figure 3A illustrates the basic configuration frequently used in one-dimensional studies of expanding plasmas (see e.g., Denavit[19]). At t=0 a semi-infinite, electrically neutral, collisionless plasma is assumed to occupy the half-space x<0. At t>0, the plasma is allowed free expansion into the vacuum domain in the positive half space x>0. As the expansion proceeds, a rarefaction wave "propagates" into the source plasma at the ion acoustic speed (top panel, 3A). The polarization field does not vary with position (middle panel, 3A), but its magnitude decreases with time. Because of this electric field, ion acceleration occurs in the bulk plasma and various levels of energized ions can be formed depending on the electron temperature.

**3.1.2 Plasma Expansion and Relevance to the Polar Wind**. *Gurevich et al.*[11a-c] *pointed out that the acceleration of ions in expanding plasmas was relevant to both space physics and astrophysics, and solar-terrestrial applications were emphasized in the work of Singh and Schunk*[12-14] *who showed the relevance of plasma expansion to the polar wind and to interhemispheric plasma flows after magnetic storms.* Singh and Schunk studied the collisionless expansion of an $H^+$ - $O^+$ -electron plasma (representing the topside ionosphere) into a vacuum (representing very low densities in the high-altitude, high L-shell plasmasphere), and followed the temporal evolution of the plasma by numerically solving the Vlasov and Poisson equations in one dimension. Figure 3B shows the initial (t=0) spatial distribution of their modeled plasma, occupying the region $-L_1 < x < 0$. They allowed the expansion to occur in the region $0 < x < L_2$. The boundary conditions on the electric field E were $E(x=-L_1)=E(x=L_2)=0$, and the initial ion velocity distributions in the source region were assumed Maxwellian.

Simulation results for the case when $H^+$ is initially a minor ion ($n(H^+)=0.1n_o$; $n(O^+)=0.9n_o$ and $T_e/T(H^+)=10$) are shown in Figure 3C. This figure shows the $H^+$ density profiles in the expanding plasma at several times $\hat{t}=tw_{pH}$ along the dimensionless spatial axis $\hat{x}=x/\lambda_{Di}$, where $\omega_{pH}$ is the $H^+$ plasma frequency and $\lambda_{Di}$ is the $H^+$ Debye length. A noteworthy feature of this expansion in the region $\hat{x}>0$ is the development of a density plateau. The extent of the plateau increases with time.

Ahead of the plateau region, the $H^+$ density decreases as expected intuitively. In and beyond the plateau region is a pure $H^+$ ion plasma, i.e., the $H^+$ ions are accelerated ahead of the expanding $O^+$ ions by the $O^+$ -electron polarization electric field that exists at the $O^+$ density front.

Figure 3D shows the energization of the light $H^+$ ions by plotting the phase-space (x-v) plots at $\hat{t}=192$. Note that the ions gain considerable velocity in the expansion region between the interface at $\hat{x}=1600$ and the lower edge of the plateau region in which the average drift velocity remains constant. Beyond the plateau region further acceleration occurs. These accelerations are caused by the electric fields set up by the expansion.

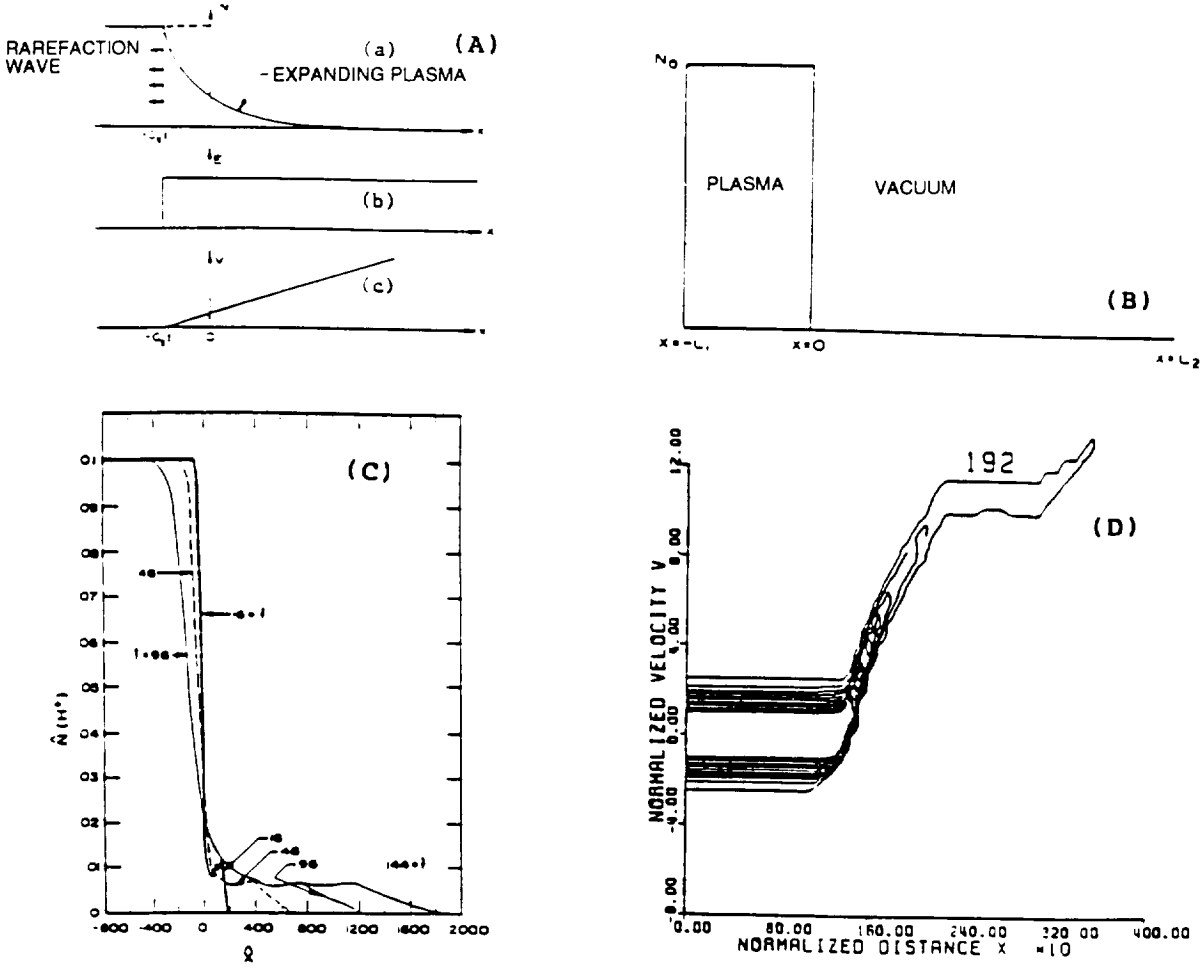


***Figure 3*** *(A) Self similar solution for the collisionless expansion of a single-ion plasma into a vacuum. The density (top), electric field (middle), and drift velocity (bottom) profiles are shown at time t; (B) Initial configuration for one-dimensional plasma expansion into a vacuum; (C) Temporal evolution of the $H^+$ density profiles for $H^+$ a minor ion and hot electrons; (D) $H^+$ phase-space plot at a selected time for $H^+$ a minor ion and hot electrons. Note that the expansion starts at $\hat{x}=1600$. (From Singh and Schunk[12])*

Singh and Schunk carried out several simulations for different compositions of the source plasma. It was found that when the light ions became the major constituent, the plateau region did not form. However, appreciable acceleration of the ions still occurred. Even the heavy $O^+$ ions underwent considerable acceleration. Simulations for various electron-to-ion temperature ratios showed that acceleration of ions up to an energy of about ten times the electron temperature was possible when the initial ion temperature satisfied the condition $T_i \leq T_e$.

**3.1.3 Relevance of Chemical Release Experiments.** Schunk and Szuszczewicz[18a] studied the very early-time (100's to 1000's of ion plasma periods) collisionless expansion of $Ba^+$, $Li^+$, and $Ba^+$- $Li^+$ plasma clouds into $O^+$ background plasmas using a one-dimensional Vlasov- Poisson model to support the polar wind simulation experiment in the CRRES mission. (The O/H and Ba/Li mass ratios in the naturally-occurring polar wind and CRRES simulation experiments are 16 and 19.79, respectively.) The following results were obtained from the numerical simulations: (1) the front of an expanding high density $Ba^+$ cloud acts as an "electrostatic snowplow," and both $O^+$ density and temperature peaks are pushed ahead of the expanding $Ba^+$ cloud; (2) the strength of the electrostatic snowplow is increased for elevated cloud electron temperatures; (3) the effect of a flowing $O^+$ background plasma (relative to the CRRES spacecraft) is to slow the $Ba^+$ expansion and change the $O^+$ response. For small $O^+$ drift velocities the $Ba^+$ snowplow still occurs; for moderate $O^+$ drift velocities ion density peaks propagate into and away from the cloud; and for large $O^+$ drift velocities the $O^+$ plasma quickly penetrates the $Ba^+$ cloud and there are small density perturbations; (4) the $Li^+$ cloud expansion is faster than the $Ba^+$ expansion by approximately the square root of the heavy-to-light ion mass ratio, and the $Li^+$ electrostatic snowplow is weaker; (5) as with a $Ba^+$ cloud, an expanding $Li^+$ cloud pushes an $O^+$ density enhancement ahead of it, but some of the light $Li^+$ ions can penetrate this $O^+$ density enhancement with the result that a $Li^+$ plateau forms and moves ahead of the propagating $O^+$ enhancement; (6) for $Li^+$ plasma expansions against a rapidly drifting $O^+$ plasma, the two plasmas quickly penetrate each other with minor density perturbations; and, (7) for a $Ba^+$ - $Li^+$ cloud expansion (simulating the $O^+/H^+$ mass ratio in the polar wind) into and $O^+$ plasma (with $Li^+$ minor), the expansion scenario is led by suprathermal forerunner $Li^+$ ions, then a propagating $Li^+$ density plateau, then a propagating $O^+$ density peak, and finally the main front of the expanding $Ba^+$ cloud.

*All of the one-dimensional plasma simulations discussed here and in previous sections are directly relevant to naturally-occurring plasma expansions as they occur without a magnetic field or along a magnetic field. Consequently, the manifestations of snowplow effects, ion discrimination, particle energization and counterstreaming flow must all be taken into account in the energy and momentum coupling process.* However, since the model does not include a magnetic field, certain wave modes, such as ion cyclotron and lower hybrid waves, cannot be excited. Therefore, even though the Vlasov-Poisson

simulations indicated that the plasma expansion scenarios considered by Singh and Schunk[12,13,14] and Schunk and Szuszczewicz [18a] were stable, the presence of a magnetic field may alter this situation. When studying the linear stability of the plasma flows, Singh and Schunk[13,14] found that the counterstreaming energetic forerunner $H^+$ ions (Figure 4C) can excite ion cyclotron waves, which in turn can thermalize and trap the energetic forerunner ions in the equatorial region. Likewise, Schunk and Szuszczewicz[18a] conducted a linear instability analysis with a constant magnetic field and showed that some of the expansion scenarios with elevated electron temperatures were unstable. When the plasma was unstable, the ion-ion acoustic wave was the most unstable mode. Depending on the conditions, waves could be excited in the expanding plasma cloud by penetrating $O^+$ ions and in the background $O^+$ plasma by penetrating cloud ions.

**3.1.4 Micro- vs Macroscopic Expansion: Lab Simulations vs Space Applications**. The Vlasov-Poisson simulations treated in previous sections correspond to very small distances (10's of cms to meters) and very early times in the expansion process (milliseconds and less). However, Singh and Schunk[82] have shown that (larger-scale) macroscopic hydrodynamic equations, when applied to the polar wind, display the same plasma expansion characteristics that are obtained from the Vlasov-Poisson equations, including ion acceleration. The reason is that in the macroscopic environment smaller polarization electric fields exist, but they extend over much greater distances and operate for longer times.

Likewise, Schunk and Szuszczewicz[18b] have conducted macroscopic hydrodynamic simulations of $Ba^+$, $Li^+$ and $Ba^+$ - $Li^+$ expansions in the F-region ionosphere (covering space/time domains of kilometers and seconds) and found expansion characteristics similar to those seen in their earlier small-scale Vlasov-Poisson simulations summarized above. The macroscale expansion scenarios were chosen to be similar to their previous small-scale short-duration numerical simulations, with the spatial and temporal scales differing by four orders of magnitude. The comparison of results not only elucidated the plasma expansion characteristics from several plasma periods to tens of seconds, but shed light on the applicability of small-scale simulations to expanding plasma clouds in the ionosphere and relevance of small-scale laboratory simulations to spaceborne applications. The macroscopic simulations showed that an expanding ion cloud can act as an electrostatic snowplow, creating a hole in the ionosphere (factor of 10) as it pushed $O^+$ density bumps (factor of 1.8) ahead of it along the geomagnetic field. For the same cloud half-width, a decrease in the cloud density led to a weaker snowplow; and an initially weaker longer-lasting snowplow ultimately produced a larger hole in the ionosphere than a short-lived strong snowplow. The simulations also showed that elevated electron temperatures act to speed the plasma cloud expansion and to strengthen the

electrostatic snowplow; and a bulk velocity component along the magnetic field had an important effect on the plasma cloud expansion and the ionospheric response. These and other macroscopic expansion features were found to run a direct parallel to those obtained from the small-scale numerical simulations.

*The important conclusion is that small-scale numerical simulations and comparably-sized laboratory experiments manifest the same physical processes and associated morphologies as those found in macroscale expansions occurring naturally in space and in the CRRES chemical-release program.* This means that for meaningful relevance to spaceborne applications, laboratory simulations should provide for scale sizes which match the very-early-time Vlasov-Poisson results of Schunk and Szuwszczewicz.[18a] Specifically, laboratory scale-size compatibility should involve the maximum physical length in the numerical simulation, characteristic minimum sizes of important phenomenologies in the expansion process, and Debye shielding distances. The maximum expansion length in the microscale simulations was 2000 dimensionless units of $\hat{x}$, where $\hat{x} = x / \lambda_{dH} = x / \left[\varepsilon_o kT_i / n_o e^2\right]^{1/2}$ and $n_o$ is the t=0 sum of cloud and background plasma densities (e.g. $n_o = n_o(Ba^+) + n_o(Li^+) + n_o(O^+)$). In the published numerical scenarios, the cloud densities ($Ba^+$ and/or $Li^+$) were typically 10 or 100 times larger than the background ionospheric $O^+$ densities. Considering F-region simulations for which $4(10^5)$ $cm^{-3} \leq N_o[O^+] \leq 4(10^6) cm^{-3}$, and assuming $1000°K \leq T_i \leq 3000°K$, the full domain of maximum expansion lengths for laboratory studies should be $22cm \leq x_{max} \leq 400$ cm. Thus a minimum requirement for laboratory chamber length is 22cm; but all scenarios within the defined parameter regime can be properly executed in a chamber 4 meters in length.

Scale considerations also include sizes of important phenemenologies and their detectability, and chamber size relative to Debye shielding distances. An important phenomenology is the minimum width of the snowplowed density "bump", which the simulations and specified parameter regimes establish at $2.2cm \leq \Delta x_{min}$ ("bump") $\leq$ 40cm. This is clearly an observable scale in a laboratory system. For electron Debye shielding distances $\lambda_D$, the selected range for $n_o$ (=sum of all charged species $=4(10^6) - 4(10^8) cm^{-3}$ with $10^3 °K \leq T_e[°K] \leq 10^4$ °K yields $1.6(10^{-3})cm \leq \lambda_D \leq 5(10^{-2})cm$. Therefore, for even the most typical chamber (e.g. 50 cm diameter), wall effects will not be a problem, as long as minimum source densities are $\geq 4(10^6)$ to $4(10^8) cm^{-3}$.

*These considerations show that high-integrity laboratory simulations can be carried out with chambers that have plasma generators with source densities in the $4(10^6)$ to $4(10^8) cm^{-3}$ regime and lengths up to at least 22 cm but preferably up to 4 meters. This will be shown to be the capability in the SAIC facilities.*

## 3.2 Related Experimental Efforts and Additional Spaceborne Considerations

That particle energization can be a manifestation of expanding plasma is not a recent discovery, for more than 50 years ago Tanberg[20] found that the cathode of a vacuum arc was the source of a supersonic plasma jet. The phenomenon was rather surprising since the ions in the jet had energies near 50 eV while the total voltage between the electrodes was only 20 volts. Since that time there have been a number of laboratory configurations that explored expanding plasma phenomena, in many cases studied with a focus on device physics. The experimental systems included vacuum arcs, laser-target interactions, exploding wires, Q-machines, triple plasma devices and simple collisional ionization e-beam sources.[20-28,74]

Most relevant to our investigation are the works of Hairapetian and Stenzel,[74] Chan et al.[25] and Wright et al.[28a] The latter efforts focused on laboratory simulations of satellite wakes in a 0.6 by 1.6m plasma chamber using an electron bombardment plasma source with an emissive wire neutralizer. The source provided a drifting Maxwellian plasma with an 18 eV drift energy and a plasma density near $10^5 cm^{-3}$ in a working nitrogen environment at $10^{-5}$ Torr. They found that the evolution of the ion stream in the wake region was consistent with theoretical expectations in the early plasma expansion works of Gurevich et al.[11a-c] and Alikhanov et al.,[11d] giving credibility (they argued) to the study of basic plasma expansion phenomena and associated processes in space vehicle wakes.

The work of Chan et al.[25] was focused on the macroscopic aspects of the self-similar specification of the expanding plasma. They measured the one dimensional time-dependent longitudinal potential profile of the expanding plasma and showed it to be self-similar. Their work was done in a filament-discharge plasma column in a small 29 cm long by 40 cm diameter chamber. They used argon with plasma densities generally greater than $10^8 cm^{-3}$ and neutral pressures greater than $10^{-5}$ Torr.

The most recent laboratory work has been that of Hairapetian and Stenzel[74] who studied the expansion of a two-electron-population plasma into a 0.8m x 1.7m chamber. They used a pulsed supersonic nozzle ($t_{on}$=1ms) to inject a collimated neutral argon beam into the ionizing path of accelerated hot-filament electrons. Their pulsed plasma source ($n_e \approx 10^{11} cm^{-3}$, $T_e^h \approx 4eV$, $T_e^h \approx 80eV$) expanded supersonically (M>2.5) into a background argon pressure of $2(10^{-6})$ Torr along an axial B-field (B≈40G). They found experimental evidence of shock-like structure and found ions accelerated to energies near 110eV. They found that during the expansion the thermal electrons ($T_e^c$) lagged behind the more energetic tail electrons ($T_c^h$) and that a strong double layer developed when the two populations separated. They offered no quantitative comparisons with

theoretical models, arguing that existing models were limited to Maxwellian plasmas and their experiment had energetic electrons with a non-Maxwellian distribution.

Contrary to the laboratory work done to date, CRRES releases were three-dimensional multi-ion expansions ($Ba^+$, $Li^+$, $Ba^+$ -$Li^+$ mixtures and others) into varying degrees of multi-ion plasmas (e.g. $O^+$, $H^+$ in the topside ionosphere). In addition, the earliest phases were collision dominated by high neutral densities, complicated by a diaphragm-venting procedure in the canisters which required 100-300ms to empty the gas into space. The releases were further complicated by plasma production terms that can include Saha thermal ionization, photoionization and critical ionization velocity effects.[75-77] In addition, there is evidence that CRRES and CRRES-like releases could have created a diamagnetic bubble in the earliest phases of expansion. While the energy density of the initial cloud ions is insufficient to produce a magnetic cavity, at early times the tight collisional coupling of the ions to the expanding cloud neutrals will allow the kinetic energy of the neutrals to be effective in creating the diamagnetic bubble. *These very early-time phenomena could never be observed in the CRRES satellite program, and therefore the complete energy and momentum coupling budget could not be taken properly into account.*

The end result of the input conditions in the actual release scenarios is a complicated "zero-order" condition of the injected plasma cloud in the spaceborne experiment. It clearly does not resemble the one-dimensional t=0 illustration of Gurevich et al.,[11] Singh and Schunk[12-14] and Schunk and Szuszczewicz,[18] nor does it resemble laboratory experiments conducted to date. *A number of these issues are addressed in this laboratory simulation with an end result that contributes a unique and complementary measurement baseline for the AMPTE and CRRES missions which sought to understand energy and momentum coupling of plasmas in the solar-terrestrial system.*

## 4. APPROACH AND RESULTS

### 4.1 The Experiment

**4.1.1 <u>Facilities and Experiment Plan</u>**. Our laboratory investigations employed a unique combination of plasma sources and diagnostic devices in medium- and large-scale vacuum chambers. We conducted high resolution measurements of expanding gas while controlling the source and background neutral gas and plasma densities. The experiments were conducted in SAIC's Space Plasma Simulation and Test Facility in McLean, Virginia, which operates the two simulation chambers illustrated in Figures 4 and 5.

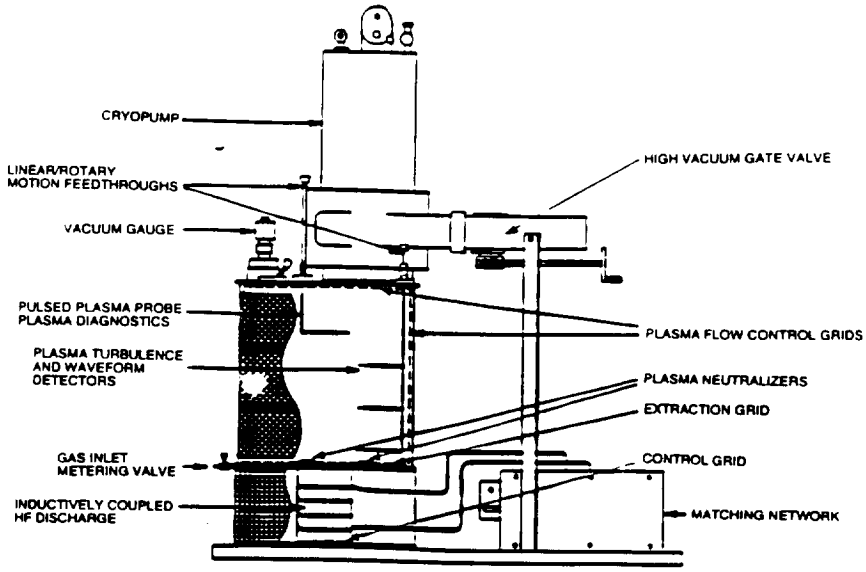


***Figure 4.*** *Plasma Expansion Chamber A*

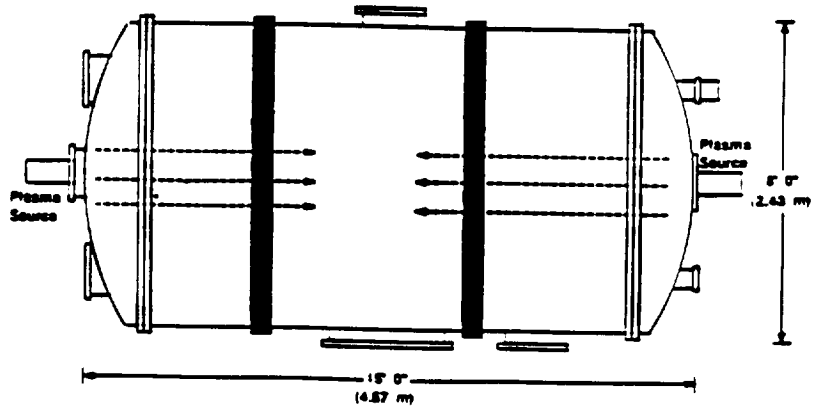


***Figure 5.*** *Plasma Expansion Chamber B*

Chamber A includes a 15 cm diameter inductively-coupled hf discharge, a 0.7 m x 1 m plasma flow chamber, a 20,000 1/s cryopump and a roughing station. The vacuum characteristics are supported by micrometer leak valves, thermocouple and cold cathode ionization gauges, and a 20" diameter gate valve. In typical operations the plasma flow and measurement capabilities are supported by four independent control grids, plasma neutralizers, and on-line diagnostics which include direct measurements of plasma density, temperature, plasma potential, mean-ion-mass, and density fluctuation power spectra. In addition, the diagnostics suite includes four channel wave analysis, with independent controls for the determination of turbulence spectra, cross-correlation functions, and three-dimensional dispersion relations. The sensors are mounted on linear and rotary-motion feedthroughs which permits mapping the plasma characteristics throughout the plasma flow volume.

The inductively-coupled plasma source is particularly versatile. With no active electrode in contact with the plasma, there are added degrees of freedom in controlling the plasma source potential and its flow characteristics. The source

is also free of the limitations typical of hot-filament type devices as well as oxide-coated-cathode discharges. Gas constituents and pressures are never a problem. The source can strike and maintain plasma discharges from $10^{-6}$ to 200 mTorr, with extrapolations to 10's of Torr readily accommodated by the system. The plasma production capabilities have a broad dynamic range with peak densities in excess of $10^{12}$ $cm^{-3}$, and higher values can be made available using the electron-cyclotron-wave resonance technique to boost densities by a factor of 50-100 [Szuszczewicz and Oechsner[48]].

Chamber A was dedicated to the first phase of experiments involving single-ion expansions into a vacuum. The noble gases were the baseline species, with He, Ne, Ar, Kr, and Xe providing ion mass selections at 4, 20.18, 39.94, 83.7 and 131.3 amu, respectively. Relative to multi-ion expansions, Xe/Ar, Ar/He, and Xe/He provide mass ratios of 3.29, 9.99 and 32.83, respectively. Parameter controls therefore included: ion mass (for a single ion expansion), ion mass ratios (for a multi-ion expansion), and source density.

Chamber B was employed in the second phase of the investigation. Chamber B, illustrated in Figure 6, is an 8' x 15' (2.43m x 4.57m), $LN_2$-lined chamber equipped with roots blower and cryopumping. It allowed for extended time- and space-domain studies of a single cloud expansion, with and without background plasma.

4.1.2 Control of Background and Expanding Plasma Characteristics. The primary device for the production of the background and the expanding plasmas was the inductively-coupled hf discharge. These sources have been operated at pressures from $(10)^{-6}$ to $(10)^{-1}$ Torr (in the published literature), with regular applications in the SAIC facility extending to 10 Torr. Typically, without a resonant enhancement,[48,78] ionization efficiencies are 0.05 to 1.0%, depending on the hf power, the gas, and the plasma confinement time. With resonance enhancement the efficiencies can extend to 100%.[78,79]

Figure 6 illustrates a configuration concept for background and source plasma creation. (We use the term "source plasma" to mean the production region or source region for the expanding plasma.) It is a generic configuration for application to Chambers A and B, allowing for the following areas of control: (a) neutral pressures identical in the source and background volume, $P_s$ and $P_b$, respectively; (b) neutral pressures impulsively greater in the source region, i.e., $P_s > P_b$, (c) no background plasma, and (d) a background plasma at a controlled fraction of the peak density in the source plasma. The gas control system independently controlled gas mixtures and pressures.

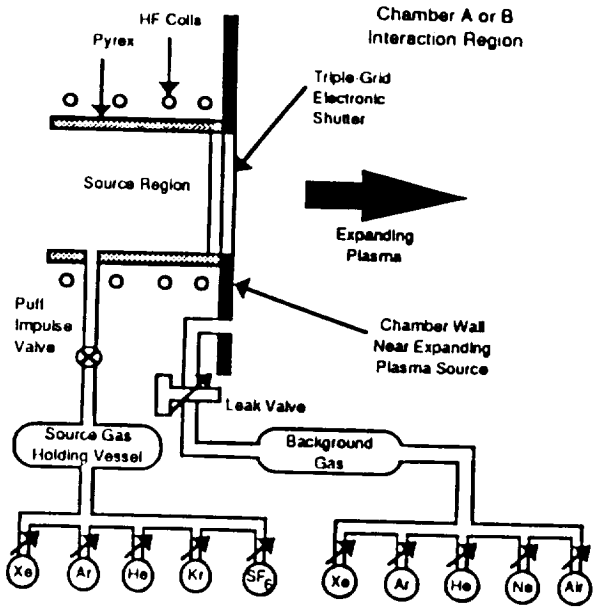


***Figure 6.*** *Schematic of Expanding Plasma Source*

4.1.3 Diagnostics. The primary diagnostics element was a pulsed plasma probe ($P^3$). The pulsed-plasma-probe is a specialized Langmuir probe technique[49-51] which overcomes the shortcomings of conventional Langmuir probes in the diagnostics of turbulent plasmas and multi-component energy distributions. The technique also provides for high-time resolution measurements of mean-ion-mass. $P^3$ heritage includes successful applications to dynamic ionospheric environments, to chemical releases in space, turbulent beam-plasma interactions in the laboratory and in the vicinity of spaceborne vehicles, to non-Maxwellian energy distributions, and to reentry plasmas.[49-61].

The $P^3$ procedure is unique in its capability for simultaneous measurements of a wide range of plasma parameters, with the simultaneity of measured parameters perhaps best illustrated in its successful application to beam-plasma interactions, an area with coupling phenomenology relevant to this investigation expanding plasmas. The work was conducted in the large vacuum facility at the Johnson Space Center using an electron beam injected into a plasma of density near $10^6$/cm.[3,58-62] $P^3$ measurements provided simultaneous multi-parameter profiles showing the spatial dependence of plasma potential, cold and suprathermal electron densities, the cold and suprathermal electron temperatures, and the spectral intensity of observed waves. These results and attendant analyses provided the first definitive measurement of copious amounts of suprathermal electrons as a function of beam-plasma parameters and as a function of position relative to the beam center. The results answered a long-standing question with

regard to the conjectured existence of the suprathermal electrons, and helped develop an understanding of the critically-important role of suprathermal electron ionization enhancements at energies below 100 eV.

### 4.2 Overview of Schedule

Experimental tasks and scheduling were driven by the scientific objectives detailed earlier with a focus on testing and validating theoretical expectations and the extrapolation of the resulting understanding and physical insight to the observational domains in the NASA/CRRES program and to analogous plasma expansion processes in the solar-terrestrial system.

We had to quantify all boundary conditions, not the least of which were the properties of the source plasma at $t<0$. This represented a minimum condition for comparison with the existing predictions, which were built upon a prescription of a one-dimensional plasma with a sharp boundary at the semi-infinite vacuum (or background plasma) half-space.

In Phase I, activities involved immediate implementation of the experiment plan using Chamber A. There were two parallel activities: the first directed at a quick view of expansion phenomenologies, morphologies and time domains, using the single-species noble-gas expansions discussed in Section 4.1.1 and the existing diagnostic complement. The parallel effort was hardware-oriented, with attention to the design and implementation of an alternative approach to the shutter electrode configuration and its gating electronics. The hardware effort included a high speed augmentation for the on-line pulsed plasma probe system and detector array. By the end of the first phase we provided initial inputs to our objectives for collisionless single-species expansion into a vacuum, with a view on the influences of source densities and gradients, collision frequencies, temperature, and ion mass.

In Phase II we transitioned our activities from Chamber A to Chamber B, so that we could explore the evolution of interactions for longer times and over larger spatial extents and parameter regimes. During this period we exploited the capabilities of Chamber B in two major types of expansion experiments. The first was the expansion of single and multi-ion plasmas into a vacuum and the second was the expansion of single- and multi-ion plasmas into a background "ionosphere". The studies in Chamber B allowed for cloud expansion measurements over a greater temporal and spatial domain while taking advantage of the chamber size and reduced influence of walls. We also dedicated the final stage of the effort to a synthesis of all experimental and theoretical work, in terms of our accumulated understanding of the expansion processes themselves and the interactive modes and acceleration processes.

## 4.3 Synopsis of Innovative Hardware Development Activities and Scientific Findings

As discussed in previous sections, the experiments were conducted in Chambers A and B within SAIC's laboratory for Atmospheric and Space Sciences in McLean, VA. Figure 7 shows a partial view of the large chamber in the foreground and the small chamber in the background, both of which were supported by on-line, computer controlled diagnostics.

***Figure 7.*** *The SAIC small and large chamber laboratory facilities employed in experimental investigation of plasma expansion phenomena.*

To tailor the existing capabilities for the expansions experiments with necessary control capabilities there were several special-purpose hardware components that had to be designed, constructed and tested. These included:

1) A supersonic nozzle to guarantee flow velocities that bounded those observed in spaceborne experiments and helped guarantee an axial flow geometry which minimized influences of reflections of the expanding gas from the side walls. To this end Mach 3.5 and 7.0 nozzles were designed using Prandle-Meyer functions and mach angles to optimize flow stability with minimum nozzle length. The nozzle designs are shown in Figure 8.

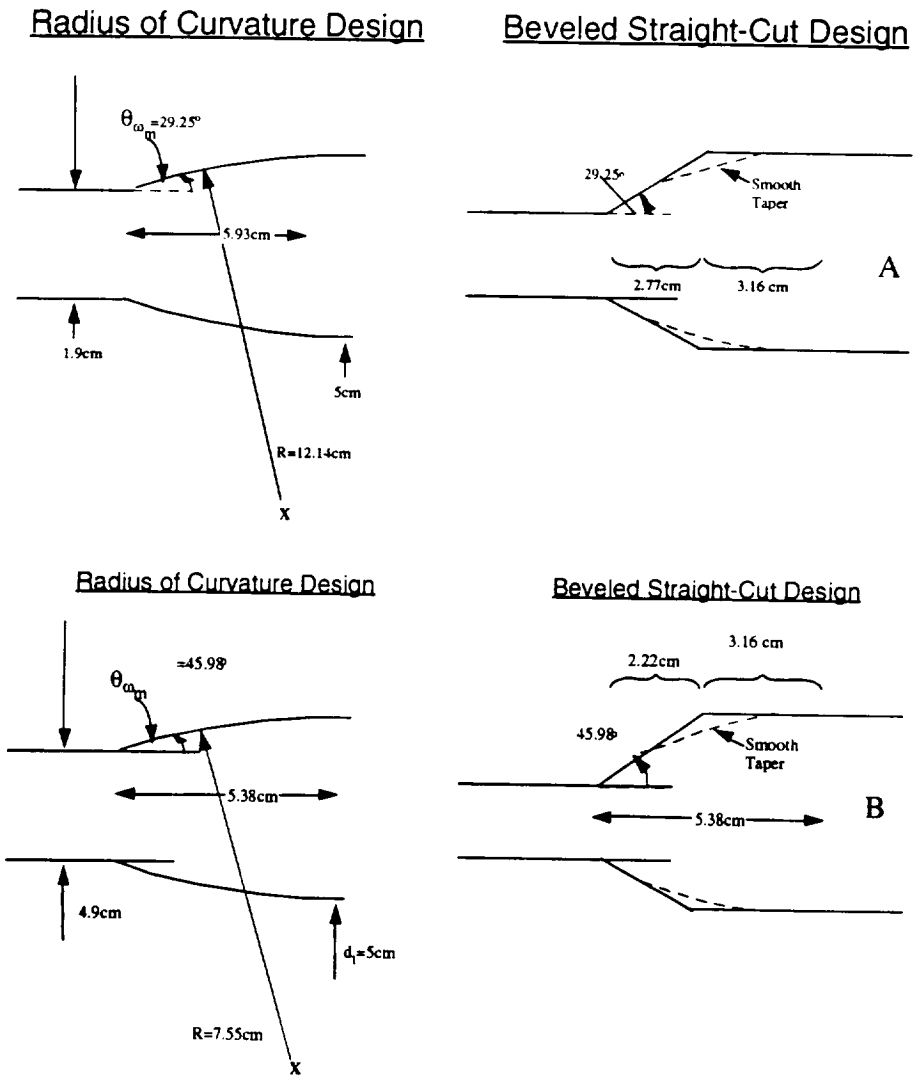


***Figure 8.*** *Supersonic nozzles (top: M=3.5; bottom M=7.0) designs employed in the investigation of plasma expansions.*

2) A sub-millisecond gas release valve which provided "burst diaphragm" characteristics, that is, an "instantaneous" gate that mimicked the simple theoretical gas release scenario (assumed in all theoretical models) contained in Figures 3A and B and allowed fast turn-around time for development of shot-to-shot comparisons and efficient overall experiment operations. The optimum design was a solenoid-activated "flapper valve" that provided a full tearing of an aluminum foil diaphragm in a submillisecond time frame. Recycle time was not less than 10 minutes nor more than 30 minutes. The "flapper valve" design is shown in Figure 9.

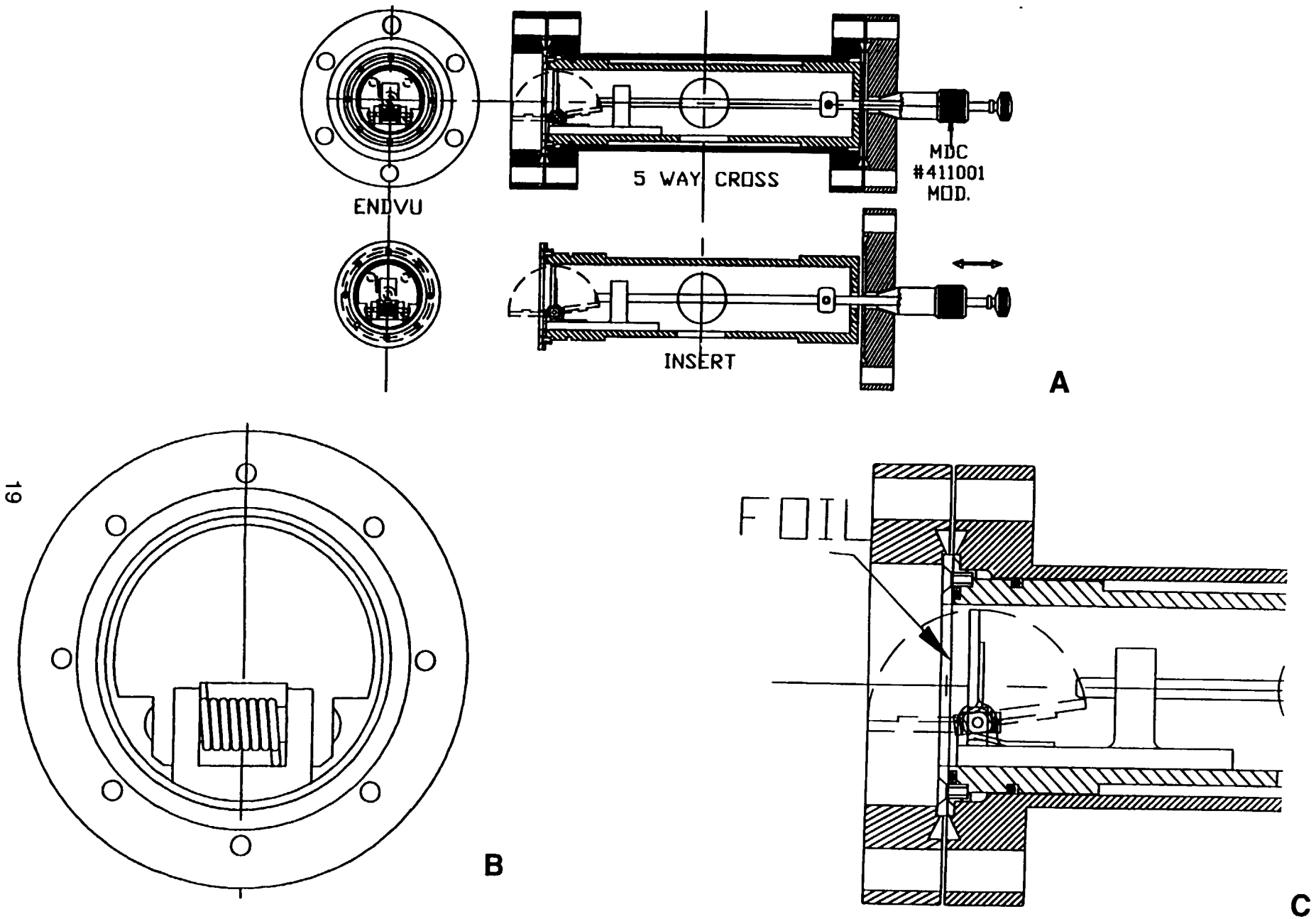




*Figure 9. The "Burst Diaphram" Gas Release Valve*

3) A gas controller and ionizer which provided the necessary reservoir of a predetermined gas mixture and then ionized it prior to "release". This guaranteed the known initial conditions of the releases allowing for the pre-release ionization component that effectively simulated the spaceborne counterparts of Saha ionization in the hot-wire mechanisms utilized in the NASA CRRES release scenarios and/or the very-early-time photo-ionization of the expanding cloud's front surface.[83] Figure 10 shows the integrated system with the gas reservoir at the bottom of the figure. Its gas mixtures were controlled by partial pressure analysis of separate gas charging lines. Pressures in the reservoir were selected to guarantee proper Mach flow characteristics through the nozzle and minimize overall chamber pumpdown time after each release. At the opening of the "flapper valve" the gas entered the hf discharge region and passed thought the nozzle into the expansion chamber (either Chamber A or B, depending on the phase of the investigation). For cases of interest involving pre-existing plasma in the expansion chamber, a background bleeder valve allowed trace gases to leak into the hf discharge region and out into the expansion chamber. With that as a pre-existing background condition the release scenario was then superimposed on that background to study the coupling processes between the expanding gas and the background "ionosphere".

4) A diagnostics array that allowed high-time resolution of the expanding cloud and its evolution of space and time. As suggested in an earlier discussion, this was achieved by a configuration of probes at several position along the cloud's expansion axis. This was done in both chambers A and B, with the chamber B configuration shown in Figure 11.

5) A time referencing device to mark the exact onset of the release so that its transit time could be checked as it passed from the nozzle to-and-through the three probe array depicted in Figure 9. This referencing was provided by two independent elements - the voltage trigger to the "flapper" valve solenoid and an optical detector which detected the onset and intensity of ionization in the hf discharge region. Those elements are not shown in any of the figures.

### 4.4 Sample Results

Figure 12 shows the time history of an expanding $A^+$ "cloud" into a simulated space vacuum with no pre-existing "ionosphere". That history is captured in terms of currents collected by probes 1, 2 and 3 in chamber B with separations from the nozzle throat at 43.3 cm, 118.8 cm and 196.9 cm, respectively. All three responses show a steep leading edge of the cloud, and intensities that suggest increasing densities (since currents are normally assumed to vary directly as charged particle currents) with increasing time and distance from the source. Figure 11 confirms that but more importantly presents the entire time history of the electron energy distribution as a function of time and position. That figure

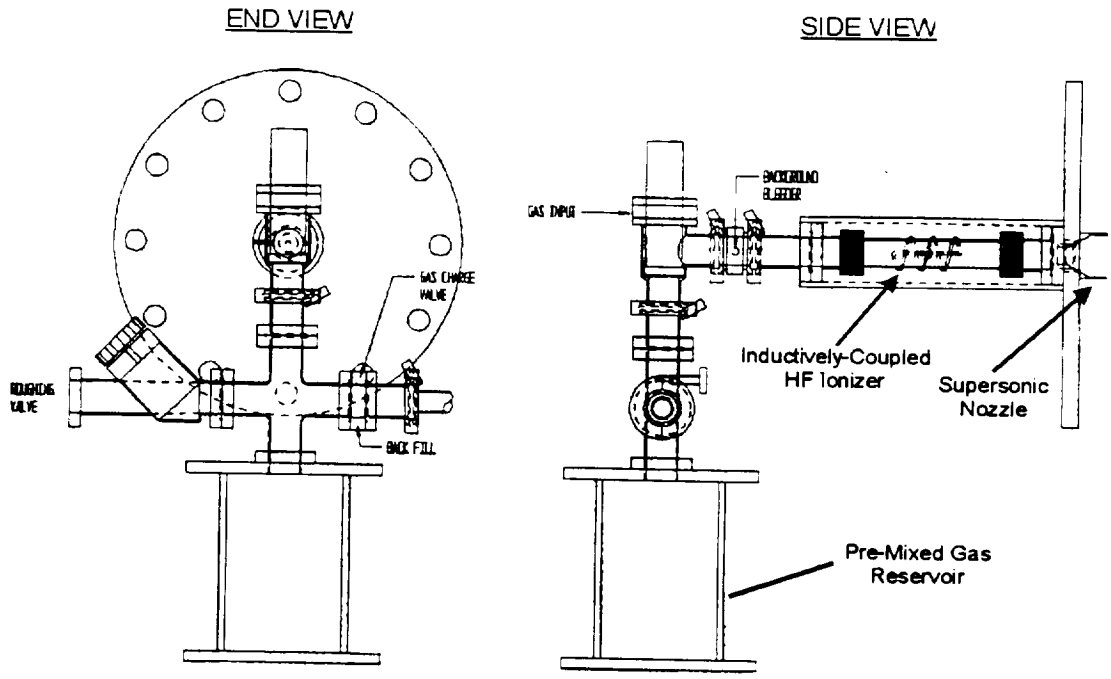


*Figure 10. Gas Handling, Ionization and Injection System*

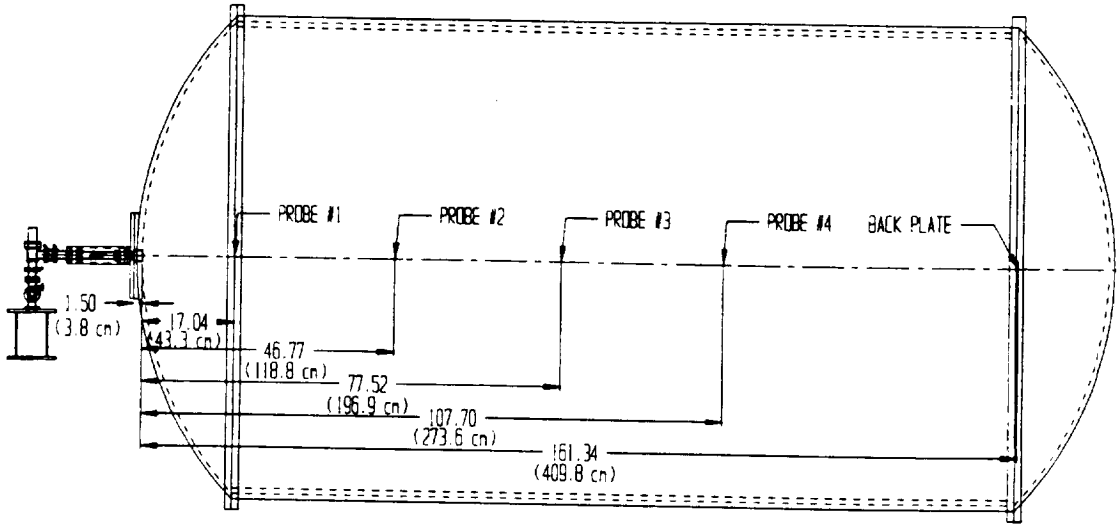


*Figure 11. Large Chamber Experiment Configuration*

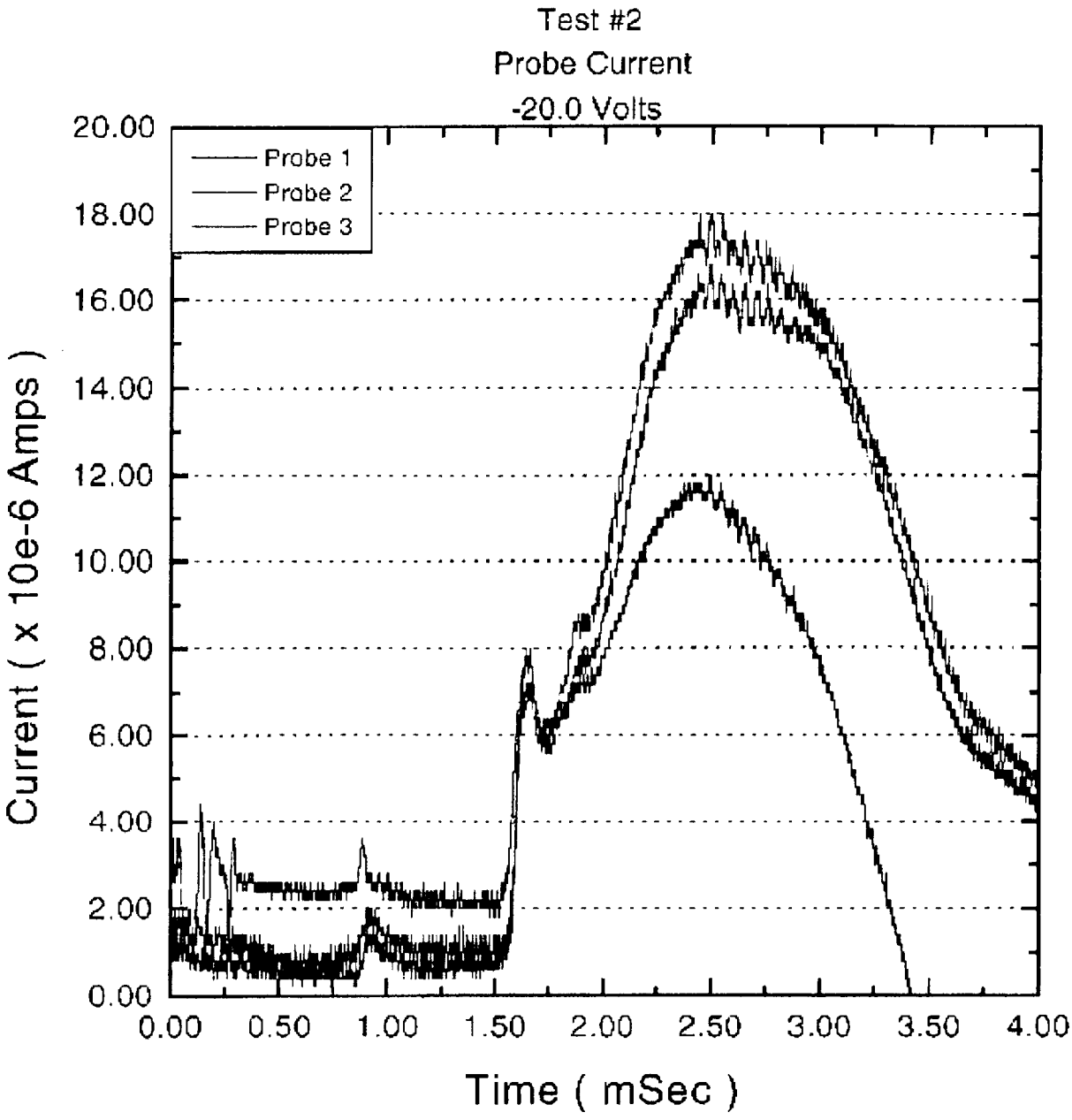


***Figure 12**. Temporal and spatial characteristics of an expanding Ar+ cloud into a simulated space vacuum with no pre-existing "background" ionosphere.*

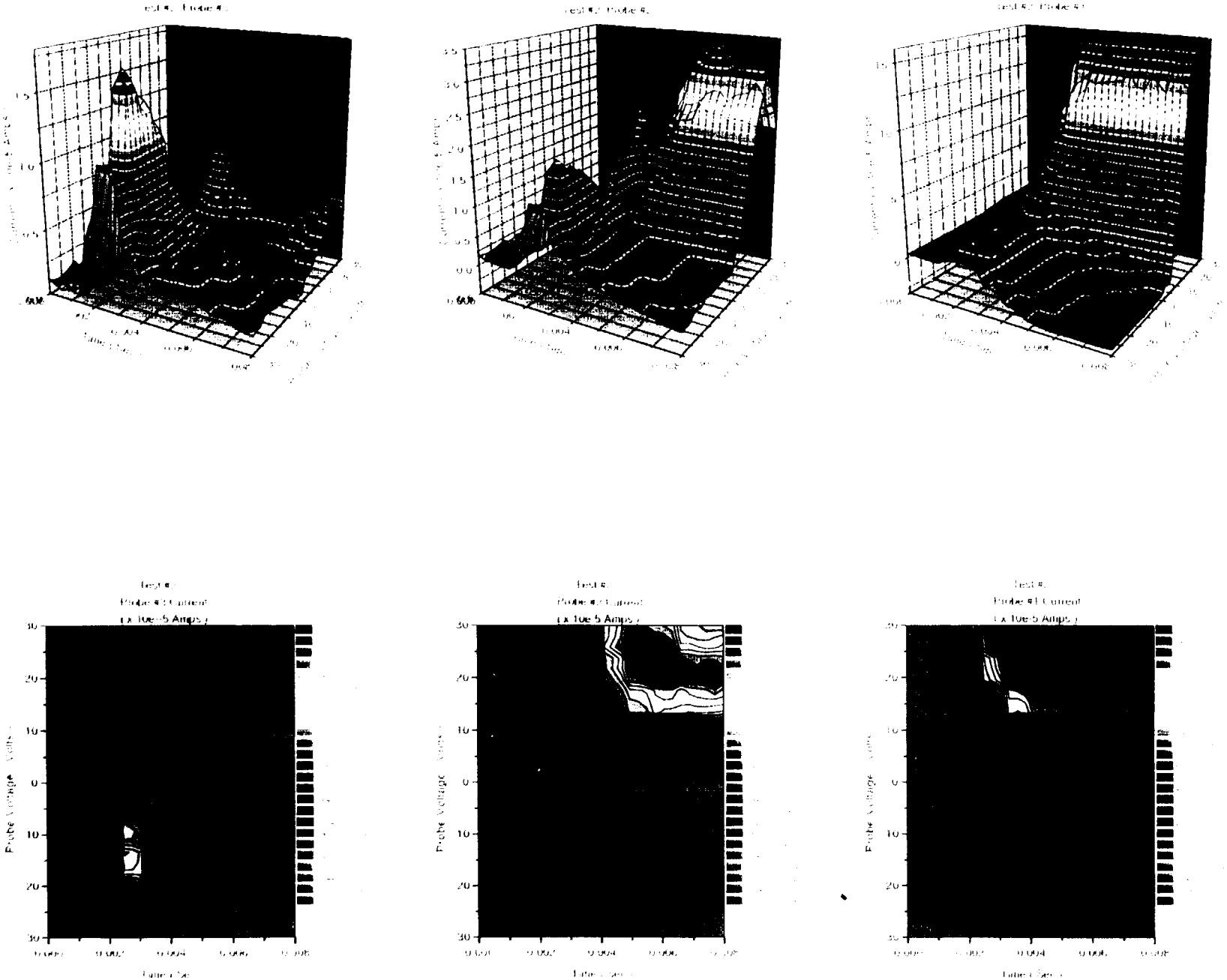

*Figure 13. Entire time histories of thermal and suprathermal electron energy distributions as a function of space and time.*

provides full I-V characteristics of each probe as a function of time, with the upper panel offering a three dimensional view of I-V vs. t, while the corresponding lower panels provide a two dimensional view of V vs. t, with color representing the magnitude. The latter presentation makes it easier to track the time-evolution of each portion of the I-V characteristic as the cloud expands.

Points to note in Figure 11:

1) Suprathermal electron tails (in the range of $-30 < V < +10$ volts) are present at all three positions in the time frame 2 - 3 ms;

2) The intensity of the suprathermal population (and the corresponding density) increases with distance from the source;

3) At later time the electron population is more Maxwellian-like, with little evidence of a suprathermal population.

This data confirms the long-theorized electron energization process in an expanding cloud. A result that was impossible to determine in spaceborne experiments (as e.g., in the CRRES program). These results provide the missing piece to previous laboratory and spaceborne programs, confirming important elements in our understanding of such solar-terrestrial processes as expanding plasmas in the solar wind (e.g., CMEs) and polar wind dynamics from the high-latitude ionospheric source region.

These signatures were seen in an entire series of runs that varied the ion species ($Ar^+$, $Xe^+$, $Kr^+$ and $Ne^+$). Correlative studies have also included spectral analyses of electrostatic waves collocated with the tail distributions. In all cases wave energies were most intense during the times in which the suprathermal populations were present with wave intensity increasing with the intensity of the suprathermal electron population. This is in keeping with theoretical expectations wherein the energization process is directly attributable to wave particle interactions. No resonance conditions (i.e., in terms of wave frequencies) were observed, with the general characteristics being relatively broadband, with power decreasing with increasing frequency.

## 5. REFERENCES

1-5. Heyvaerts, J., in Solar Flare Magnetohydrodynamics, E.R. Priest, editor, Gordon and Breach, p. 429 (1981); Rosner, R. et al., in Solar Terrestrial Physics: Present and Future, NASA Ref. Publ. 1120 (1984); Singh, et al., Physica Scripta 33, 355 (1986); Stone, N.H., NASA Tech. Paper 1933 (Nov. 1981); Sach, Ch. and H. Schamel, Phys. Reports 156, 311 (1987).

6-7. Szuszczewicz, E.P., in Space Technology Plasma Issues in 2001, H. Garret, et al., eds. JPL Publ. 84-49 (1986); Szuszczewicz, E.P., et al., AIAA J. (1988).

8-10. Arons, J., Space Science Rev. 24, 437 (1979); Axford, W.I., in Plasma Astrophysics, Guyenne and Levy, editors, ESA SP-161, p. 427 (1981); Forman, M.A., et al., Sov. Phys. JETP 32, 1061 (1971).

12-15. Singh and Schunk, J. Geophys. Res. 87, 9154; Singh, and Schunk, Phys. Fluids 26, 1123, (1983a); Singh and Schunk, J. Geophys. Res. (1983b); Schunk and Watkins, J. Geophys. Res. 87, 171 (1982);

16-17. Parks, C. G., J. Geophys. Res. 75, 4249, (1970); Bailey, G.J., et al., Planet. Space Sci. 26, 753, (1978).

18a-c. Schunk and Szuszczewicz, J. Geophys. Res. 93, 12901 (1988); Schunk and Szuszczewicz, J. Geophys. Res. 96, 1337 (1991); Earle, et al., SAIC Rpt. (1989).

19-21. Denavit, J., Phys. Fluids 22, 1384 (1979); Tanberg, R., Phys. Rev. 35, 1080 (1930); Hendel and Reboul, Phys. Fluids 5, 360 (1962).

22-24. Goldenbaum and Gerber, Phys. Fluids 16, 1289 (1973); Begay, and Forslund, Phys. Fluids 25, 1675 (1982); Korn, P., et al., Phys. Fluids 13, 517 (1970).

25-27. Chan, et al., Phys. Fluids 27, 266 (1984); Wieckert, C., Phys. Fluids 30, 1810 (1987); Aithal, et al., Phys. Fluids 30, 3825 (1987).

28a-b. Wright, et al., J. Plasma Phys. 33, 71 (1985); Stone, et al., Geophys. Res. Lett. 15, 1169 (1988).

29-30. Sjolander and Szuszczewicz, J. Geophys. Res. 84, 4393 (1979); Daly and Whalen, J. Geophys. Res. 84, 6581 (1979).

31a-b. Marklund, et al., J. Geophys. Res. 92, 4590 (1987); Eliasson, et al., Adv. Sp. Phys. 8, (1)93 (1988).

32-33. Kelley, et al., J. Geophys. Res. 85, 5055 (1980); Holmgren, et al., J. Geophys. Res. 85, 5043 (1980).

34a-b. Luhr, et al., J. Geophys. Res. 91, 1261 (1986); Ma, et al., J. Geophys. Res. 92, 2555 (1987).

35-42. Paschmann, et al., J. Geophys. Res. 91, 1271 (1986); Hausler, et al., J. Geophys. Res. 91, 1283 (1986); Gurnett, et al., J. Geophys. Res. 91, 1301 (1986); Coates, et al., J. Geophys. Res. 91, 1311 (1986); Hall, et al., J. Geophys. Res. 91, 1320 (1986); Mobius, et al., J. Geophys. Res.

91, 1325 (1986); Liu, et al., J. Geophys. Res. 91, 1333 (1986); Krimigis, et al., J. Geophys. Res. 91, 1339 (1986).

43-45. Szuszczewicz, E.P., J. Atm. Terr. Phys. 47, 1189 (1985); Szuszczewicz, et al., J. Geophys. Res. 87, 1565 (1982); Szuszczewicz, E.P., AIAA J. 21, 1374 (1983).

46-47. Gekelman, et al., J. Geophys. Res. 87, 101 (1982); Stenzel, et al., J. Geophys. Res. 87, 111 (1982).

48. Szuszczewicz and Oechsner, J. Appl. Phys. 42, 4974 (1971).

49-52. Holmes and Szuszczewicz, Rev. Sci. Inst. 52, 377 (1981); Szuszczewicz and Holmes, J. Appl. Phys. 46, 5134 (1975); Szuszczewicz and Holmes, Rev. Sci. Instr. 46, 592 (1975); Szuszczewicz and Holmes, AIAA Paper No. 76-393, AIAA 9th Fluid and Plasma Dynamics Conference (San Diego, CA, July 1976).

53-55. Szuszczewicz, et al., Geophys. Res. Lett. 6, 201 (1979); Singh and Szuszczewicz, J. Geophys. Res. 89, 5575 (1984). Szuszczewicz, et al., Astrophy. and Sp. Sci. 86, 235 (1982).

56-58. Narcisi and Szuszczewicz, ESA SP-195, 299 (1983); Sjolander and Szuszczewicz, J. Geophys. Res. 84, 4393 (1979); Szuszczewicz, E.P., et al., in Active Experiments in Space, (G. Haerendel, ed.) ESA-195, Netherlands, (1983).

59-61. Szuszczewicz, E.P., et al., Geophys. Res. Lett. 6, 201 (1979); Szuszczewicz, E.P., et al., in Active Experiments in Space, (G. Haerendel, ed.), ESA SP-195, 189, (1983); Szuszczewicz, E.P., AIAA Journal 21, 1374 (1984).

62-69. Stenzel, et al., Rev. Sci. Instr. 54, 1302 (1983); Gekelman and Stenzel, Phys. Rev. Lett. 54, 2414 (1985); Stenzel, et al., Rev. Sci. Instr. 53, 1027, (1982); Stenzel, et al., J. Geophys. Res. 88, 4793 (1983); Stenzel, et al., Rev. Sci. Instru. 54, 1302 (1983); Urrutia and Stenzel, University of California, Los Angeles, Plasma Physics Group Report PPG-681, Feb. 1983; Whelan and Stenzel, Phys. Rev. Lett. 50, 1133, (1983); Urrutia and Stenzel, University of California, Los Angeles, Plasma Physics Group Report PPG-688, March 1983.

70-72. Szuszczewicz, et al., Annales Geophys. 6, 3(1988); Schunk and Szuszczewicz, Annales Geophys. 6, 19 (1988); Szuszczewicz, et al., Chang and Crew, eds., (1988 in press).

73. Ma, et al., J. Geophys. Res. 92, (1987).

74. Hairapetian and Stenzel, Phys. Rev. Lett. 61, 1607 (1988).

75-77. Alfven, H., Oxford Univ. Press (New York, 1954); Machida, et al., Phys. Fluids 27, 1928 (1984); Machida and Goertz, J. Geophys. Res. 91, 11976 (1986).

78-80. Boswell, R.W., Plasma Physics and Controlled Fusion 26, 1147 (1984); Boswell and Porteous, Applied Phys. Lett. 50, 1130 (1987); Cross and Valentini, Rev. Sci., Instrum. 53, 38 (1982).

81-82. Szuszczewicz, et al., Astrophys. and Sp. Sci. 66, 235 (1982); Singh and Schunk, J. Geophys. Res. 90, 6487-6496 (1985).

83. Szuszczewicz, et al., J. Geophys. Res. (1996 in press).